Green synthesis of graphitic nanobiochar for the removal of emerging contaminants in aqueous media

Sammani Ramanayaka [a], Daniel C.W. Tsang [b], Deyi Hou [c], Yong Sik Ok [d,*], Meththika Vithanage [a,*]

[a] Ecosphere Resilience Research Center, Faculty of Applied Sciences, University of Sri Jayewardenepura, Nugegoda, Sri Lanka
[b] Department of Civil and Environmental Engineering, The Hong Kong Polytechnic University, Hung Hom, Kowloon, Hong Kong, China
[c] School of Environment, Tsinghua University, Beijing 100084, China
[d] Korea Biochar Research Center, O-Jeong Eco-Resilience Institute (OJERI) & Division of Environmental Science and Ecological Engineering, Korea University, Seoul 02841, South Korea

HIGHLIGHTS

- Graphitic flaky nanobiochar was formed by top-down approach through disc milling.
- Aggregation of nanobiochar was prominent and seen well in scanning electron imaging.
- Glyphosate, oxytetracycline, Cr(VI), Cd sorption were pH dependent and cooperative.
- Partition coefficient data depicted nanobiochar's capacity in removing contaminants.

GRAPHICAL ABSTRACT

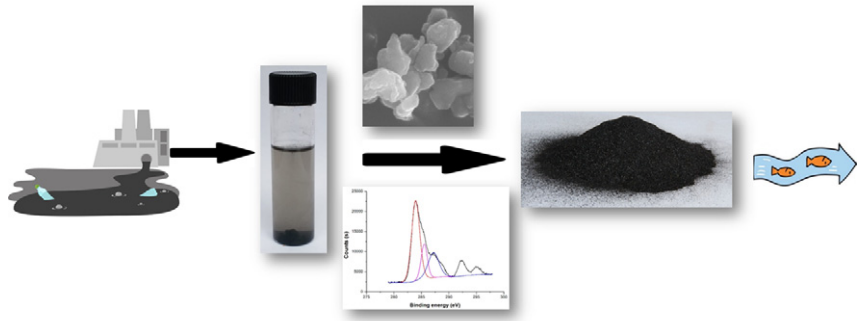

ARTICLE INFO

Article history:
Received 18 September 2019
Received in revised form 21 November 2019
Accepted 22 November 2019
Available online 28 November 2019

Keywords:
Potentially toxic elements
Nanomaterials
Environmental remediation
Mechanical grinding
Facile synthesis

ABSTRACT

This study reports the preparation of nanobiochar (NBC) via top-down approach of bioenergy waste-derived dendro biochar through mechanised grinding in order to assess its capacity to remove emerging contaminants, such as antibiotics, agrochemicals, and potentially toxic elements from aqueous media. Preconditioned biochar was disc milled in ethanol media, and the resulting colloidal biochar was dispersed in water to obtain the NBC fraction by centrifugation. Adsorption edge and isotherm experiments were carried out at pH 3 to 8 and NBC dosages of 0.5 g/L for oxytetracycline (OTC), glyphosate (GL), hexavalent chromium (CrVI), and cadmium (CdII). NBC was characterised by scanning electron microscopy, X-ray photoelectron spectroscopy, Brunauer–Emmett–Teller surface area, and Fourier transform infrared spectroscopy, which demonstrated the flakey and graphitic nature of the NBC particles with a surface area of 28 m^2/g and the presence of different functional groups, such as —OH, C═O, —NH, and CH_3. The best pH for OTC and Cd(II) was 9, whereas the best pH levels for GL and Cr(VI) were 7 and 4, respectively. Isotherms depicted a positive cooperative adsorption mechanism by providing the best fit to the Hills equation, with high removal capacities for four contaminants. Dendro NBC showed the best performance, demonstrated by the high partition coefficient for the removal of OTC, GL, Cr(VI), and Cd(II) over various types of adsorbents. The overall results indicated that graphitic NBC produced by mechanical grinding of dendro biochar is a promising material for the removal of OTC, GL, Cr(VI), and Cd(II) from aqueous media.

1. Introduction

Biochar, a carbonaceous material, is an alternative sorbent for pollution remediation owing to its outstanding adsorption properties, comparatively low cost, and environmental compatibility (Lyu et al., 2018). Biochar characteristics and yields vary according to the feedstock type, temperature, production technique, and pre/post-modification. Municipal solid waste, agricultural waste, and wood are some of the materials that can be used as feedstock in pyrolysis (Ashiq et al., 2019). Slow pyrolysis in an oxygen-free environment results in a large quantity of biochar while producing a small amount of bio-oil (Mohan et al., 2014). High biochar yield can be obtained from wood, while comparatively low yield is obtained from municipal solid waste (Ashiq et al., 2019). Among the various applications of biochar, its role as an adsorbent has received significant attention owing to its high capacity.

The sorption properties of biochar have been studied for the removal of various organic and inorganic contaminants, including pharmaceuticals and personal care products, pesticides, steroid hormones, and potentially toxic metals in aqueous media (Taheran et al., 2018). These micropollutants, known as emerging contaminants (EC), are released into the natural environment by anthropogenic activities such as wastewater discharge, improper waste disposal, and direct application of agrochemicals in agricultural lands. In the case of pharmaceuticals such as antibiotics, >70% of the active form of the drug is excreted via bodily secretions, urine, and faecal matter (Daghrir and Drogui, 2013). The development of antibiotic resistance in humans, carcinogenic properties, and the persistence of potentially toxic elements (PTEs) in living organisms that cause various disorders have made these specific ECs highly unsafe for the environment. Tetracyclines (TC), one of the most commonly used antibiotic groups in the livestock industry, accounts for nearly 32% of total veterinary antibiotic consumption (Agency, 2017). Therefore, the amount of antibiotics discharged into the natural environment has progressively increased. The concentrations of oxytetracycline (OTC) in aquatic environments exceed the limit set by the World Health Organization (<1 μg/L; WHO, 2012). Surface water samples from a river around large-scale livestock farms in the Chinese province of Jiangsu showed a maximum OTC concentration of 73 μg/L (Wei et al., 2011). Regarding agrochemicals, glyphosate (GL) is one of the most widely used herbicides around the world. Although the United States Environmental Protection Agency has listed GL as a category II toxic chemical, with a maximum limit of 0.7 μg/L in drinking water, it is detected at extremely high concentrations in the range of 1200–1500 μg/L in water bodies (Mayakaduwa et al., 2016).

Toxic metal ions, known as potentially toxic elements (PTEs), can accumulate in aquatic environments and soils due to accidental discharge of industrial effluents. Among many PTEs, hexavalent chromium Cr(VI) has been identified as one of the most toxic trace metal pollutants since it can penetrate throughout the skin and affect the central nervous system and respiratory system. In some cases, the amount of Cr(VI) detected in water is 2000 μg/L, which exceeds the WHO limit of 50 μg/L (Asfaw et al., 2017). During their removal, hexavalent chromium ions are reduced to the nontoxic trivalent form of chromium [Cr(III)] using a reducing agent. Similar to Cr(VI), cadmium [Cd(II)] exhibits acute toxic effects on the kidneys, causing irreversible damage. Cd(II) contamination of aquatic environments has been detected in the range of 0.1–0.5 mg/L, while the WHO has set a maximum Cd(II) concentration of 0.003 mg/L owing to its extreme toxicity (Sohi et al., 2010). Therefore, since it is essential to remove these anthropogenic pollutants from water, biochar has received recent attention as a SMART material for environmental remediation over other adsorbents such as activated carbon due to the lower cost of production, unique properties, and carbon negativity (Rajapaksha et al., 2016). Among the various biochars that have been examined for environmental remediation, woody biochar received specific attention since it is produced by power plants as a by-product and possess a high capacity to remove various different contaminants (Mayakaduwa et al., 2016; Herath et al., 2015).

Biochars are subjected to both chemical and physical modification methods. The chemical modification includes oxidation, acid/base treatment, CO_2 activation, and coating. However, physical modification methods have not received sufficient attention from researchers (Lyu et al., 2018). In the literature, ball milling has been proposed as the most appropriate method for the preparation of nanobiochar (NBC) to improve its properties (Fan et al., 2016). Although various ball milling methods have been used to produce NBCs, to the best of our knowledge, double-disc milling has not been applied for NBC preparation may be due to the high cost of operation. However, it is found that the vibration disc milling is better to obtain a uniform size and shape and to increase the quantity of NBC through shear and attrition stress compared to ball milling, which is the most commonly used (Bayram and Öner, 2007; Karinkanta et al., 2018). In the case of ball milling, grinding occurs due to colliding particles, which may tend to aggregate, increasing the apparent particle size (Bayram and Öner, 2007; Karinkanta et al., 2018). Moreover, few studies have assessed engineered NBCs for environmental remediation and obtained promising results. However, these investigations utilised various types of NBCs and were limited to specific organic compounds and metal/loids such as carbamazepine, phenanthrene, As, and Ni (Lian et al., 2018; Lyu et al., 2018; Naghdi et al., 2017b; Nath et al., 2019). As far as we know, no studies are reported in the literature on the use of NBCs produced by double-disc milling for a wide range of contaminant removal. At the same time, since experimental conditions are different, it is inappropriate to compare the studies through their capacities (Vikrant and Kim, 2018). Hence, partition coefficient (PC) was calculated to compare it with that obtained in previous studies, where data for NBC is lacking. Therefore, the objectives of this study are to examine the preparation of NBC by double-disc milling and to test its universal performance and applicability for the removal of various contaminants such as antibiotics, herbicides, and PTEs.

2. Materials and methodology

2.1. Chemicals

Oxytetracycline (OTC; HPLC grade, 95%), cadmium nitrate [$Cd(NO_3)_2$; analytical reagent, 99%], Glyphosate (GL; analytical Standard, 99%), potassium dichromate [$K_2(Cr_2O_7)$; analytical reagent, 99.5%], ninhydrin (analytical reagent, 99%), citric acid (analytical reagent, 99.5%), diphenylcarbazide (DPC; analytical reagent, 97%), 14.6 M H_3PO_4 (extra pure AR, > 85%), and acetone (extra pure AR, 99.5%) were purchased from Sigma-Aldrich Co. Ltd. (United States). Nitric acid (HNO_3) and sodium hydroxide (NaOH) were used to regulate the solution pH.

2.2. Preparation of biochar

Woody biochar, a byproduct of *Gliricidia sepium* gasification, was collected from the dendro thermal power plant in Thirappane, Sri Lanka. The biochar was crushed into pieces, sieved (< 3 mm), washed with distilled water, and oven-dried for 24 h at 60 °C. Thereafter, it was preconditioned at −80 °C for three days and mechanically grounded using a disc mill (Siebtechnik TS 250, Germany; Naghdi et al., 2017a). Dried biochar, mixed with ethanol, was subjected to disc mill grinding for 2 min at 1000 rpm (Peterson et al., 2012). The resulting colloidal biochar (5 g) was dispersed in 100 mL of ethanol and centrifuged at 2000 rpm for 10 min. The supernatant, which contained the nano fraction of biochar, was collected, sonicated at 50 kHz for 30 min (Elmasonic S, Germany), and dried in Petri dishes using a vacuum oven at 50 °C (Eyela NDO, Japan). The dried layer of NBC was scraped off with a spatula and collected for characterisation and adsorption experiments Fig. 1.

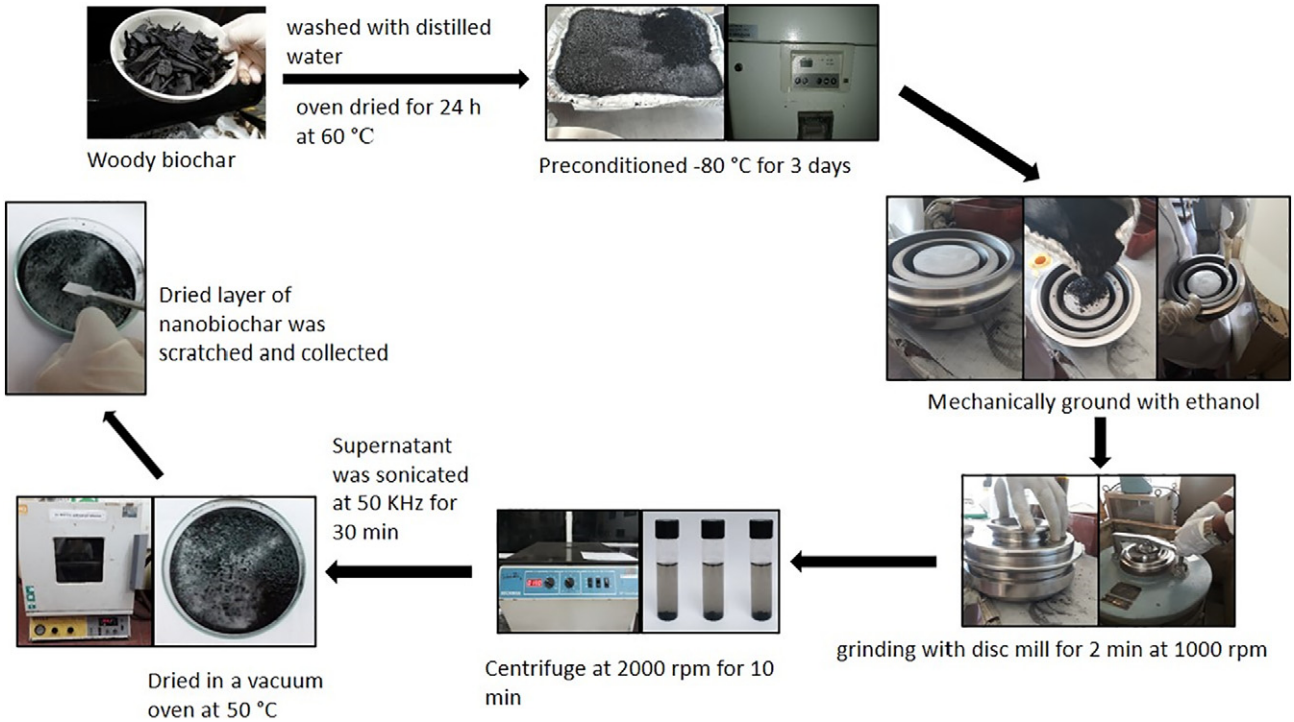

Fig. 1. Production procedure of nanobiochar preparation using double-disc mill.

2.3. Characterisation of biochar

The surface morphology of NBC was investigated by Field-Emission Scanning Electron microscopy (FE-SEM; Hitachi SU6600, Japan). The surface chemistry of NBC was investigated by X-ray Photoelectron Spectroscopy (XPS), using a Kratos Axis 165 electron spectrometer with a monochromatised Al X-ray source at 12 mA and 14 kV. Survey scans spanning binding energies from 1100 to 0 eV were collected with an analyser pass energy of 160 eV and a step of 0.3 eV (ESCALABXi, Thermo Scientific, USA). A nanoparticle analyser (Horiba SZ-100, Japan) was used to analyse the size of NBC particles. The mineral constituents in the biochar structure were determined by Powder X-ray Diffraction (PXRD - Rigaku Ultima IV X-ray Diffractometer, Japan) patterns using Cu Kα radiation at a wavelength of 1.54056 Å, scanning range of 10–60° (2θ), and scanning speed of 2° per min. Surface functional groups of biochar were determined by Fourier Transform Infrared Spectroscopy (FTIR, Thermo Scientific Nicolet iS10, USA) in the wavelength range of 4000–550 cm^{-1}. Solution pH values were measured with a pH meter (Adwa AD1030, Romania). The Brunauer–Emmett–Teller (BET) surface area analysis of NBC was conducted using the Autosorb-iQ-MP/XR (Quantachrome, Germany).

2.4. Edge experiments

A suspension of NBC was hydrated for 4 h on a magnetic stirrer purging high-purity nitrogen for 30 min. The concentrations of OTC, GL, Cr (VI), and Cd(II) were maintained at 25, 20, 5, and 10 mg/L, respectively, in a solid solution at an initial NBC dosage of 0.5 g/L. The adsorption pH was studied in the range of 3.0–9.0, and the solution pH values were adjusted using HNO_3 and NaOH (0.1 mol dm^{-3}). The adsorption process was carried out overnight in a shaker at 100 rpm. Finally, the suspensions were filtered through a 0.45 μm syringe filter. The absorbance values of the resulting solutions of OTC and Cd(II) were measured at wavelengths of 356 and 228.8 nm using a UV–Vis spectrophotometer (Shimadzu UV160A, Japan) and Atomic Absorption Spectrometer (AAS - iCE3000, Thermo Scientific, USA), respectively. Colour development procedures were carried out to measure GL and Cr(VI) concentrations. To develop the purple colour in GL, ninhydrin (1 mL) and citric acid (1 mL) were added to 0.4 mL of sample, and the volume was increased to 10 mL. The solution was kept in a hot water bath (95 °C) for 12 min, and absorbance values were measured at 570 nm using a UV–Vis spectrophotometer (Mayakaduwa et al., 2016). For Cr(VI), a fresh solution of DPC was prepared using 1,5-DPC (0.0114 g) dissolved in acetone (3 mL) and 16.4 M H_3PO_4 (3.6 mL). Deionised water was added until a final volume of 15 mL was obtained. Then, the prepared DPC solution (1 mL) was added to 2 mL of sample, and the volume rose to 10 mL. The solution was left for 20 min to develop a pink-violet colour. Absorbance values were then measured at 540 nm using the UV–Vis spectrophotometer (Rajapaksha et al., 2018).

2.5. Isotherm experiments

Isotherm experiments were carried out at a room temperature of 303 K (30 °C) to assess the effect of initial adsorbate concentrations on the best pH value identified from the edge test. OTC concentrations were maintained at pH 4.75 in the range of 10–500 mg/L for adsorption isotherm experiments at 1 g/L adsorbent dosage. GL concentrations were in the range of 5–250 mg/L, and samples were pipetted out at the best adsorption pH of 6.0. Hexavalent chromium exhibited the best adsorption at a pH of 3.75, and the concentration range was from 1 to 25 mg/L. Cd(II) concentrations were maintained in the range of 5–300 mg/L at pH 7.0. After 4 h of hydration and contact time of 12 h, i.e., the time needed to reach equilibrium, the solid solutions were centrifuged at 2000 rpm for 10 min. Finally, the supernatant was filtered using a 0.45 μm syringe filter and analysed using the UV–Vis spectrophotometer and atomic absorption spectrometer at the specified wavelength values for each adsorbate. For Cr(VI) and GL, colour development steps were carried out as mentioned above. The adsorbed amount q_e (mg/g) was determined by Eq. (1)

$$q_e = \frac{C_c - C_s}{C_{NBC}} \quad (1)$$

where q_e is the amount of OTC, GL, Cr(VI), and Cd(II) adsorbed onto NBC; C_s is the adsorbate concentration (mg/L) in the supernatant of the sample; C_c is the adsorbate concentration (mg/L) in the control; and C_{NBC} is the NBC concentration (g/L).

Origin 6.0 software was used for isotherm data modelling using the Hills, Freundlich, Langmuir, Temkin, and Redlich–Peterson equations (supplementary materials) to evaluate the maximum adsorption capacities of OTC, GL, Cr(VI), and Cd(II) with equilibrium time. The maximum adsorption capacity and equilibrium time of NBC were determined with best-fit curves. The isotherm model, which yields the best-fit curve, and the correlation coefficient (R^2) with value closest to +1, were selected.

3. Results and discussion

3.1. Characterisation of NBC

The BET specific surface area was recorded as 28 m^2/g, which was determined using the Barrett, Joyner, and Halenda method. It is about 10 folds less than that of the pristine macro-scale biochar, which may be due to the collective account of macro, meso, and micropores. Although the surface area depends on the nanoparticle synthesis method, it was found that the surface area resulting from disc milling was in the lowest range of NBC values compared to those reported in the literature at 5–370 m^2/g, which may be attributed to the graphitic nature and the presence of nanopores (Lyu et al., 2018; Naghdi et al., 2019, 2017a; Weber and Quicker, 2018).

3.1.1. Scanning Electron microscopic analysis

The micrographs of NBC captured at two different magnifications (×6.00 and ×70.0 k) are shown in Fig. 1. The flakey structure of NBC particles (Fig. 1b) was discovered with length and diameter of <1 μm and 50–150 nm, respectively. Most particles exhibit a polygonal shape (Naghdi et al., 2017a). Due to static charges among NBC particles, agglomeration can be perceived (Fig. 2a and b).

3.1.2. Powder X-ray diffraction analysis

Amorphous characteristics and some minerals such as silicon dioxide (SiO_2) and calcium carbonate ($CaCO_3$) were identified from the PXRD pattern of NBC with a calcite phase (Fig. 3a). The peaks illustrate the characterisation index of the NBC peaks (104), (113), (202), and (116) with diffraction angles of $2\theta = 29.32°$, 39.33°, 43.08°, and 48.43°, respectively.

3.1.3. Fourier transform infrared spectroscopic analysis

Pristine dendro biochar depicts a few strong, sharp, and broad peaks in the FTIR spectrum, which clarifies its surface functional groups. The robust and broad peak at 3420 cm^{-1} was designated as phenolic —OH stretching while the shoulder at 1655 cm^{-1} showed the NH bend of primary amines (Xu et al., 2011). Sharp peaks at 1420 cm^{-1} and 1384 cm^{-1} expressed C═O ketone and CH_3 bend, respectively (Herath et al., 2015). A broad Si—O stretching was found at 1092 cm^{-1}, and a sharp peak of aromatic C—H out-of-plane deformation was observed around 873 cm^{-1}, which condensed the small aromatic units into large sheets (Fig. 3b.

3.1.4. X-ray photoelectron spectroscopy

The X-ray photoelectron spectroscopy analysis indicated the presence of C, O, and N as the main elements (>85%) on the NBC surface, while Ca, Mg, Si, and S were also present as minor elements. The overall XPS spectrum of NBC is shown in Fig. S1. The spectra C 1s indicates three different peak types with different binding energy values, which can be assigned to sp. 2C and sp. 3C: (C—I) highly ordered pyrolytic graphitic C—C at 283.9; (C—II) C—O, C—H, and C—N due to the presence of phenolic, alcohol, and ether at 285.5; and (C—III) O═C—O or C—N confirmed at 287.3 eV (Bian et al., 2015). Only one O 1s peak appeared in the NBC spectra, which corresponds to the binding energies of O—II C═O at 530.9 eV (Sitko et al., 2013). However, biochar contains 2 O 1s peaks, whereas NBC has a single peak with no O—H peak, indicating the absence of water owing to the use of ethanol for milling. The high binding energy regime of the C 1s spectra is approximately 292 eV, which may have resulted from the energy loss of the outgoing photoelectrons for $\pi \rightarrow \pi^*$ transition in XPS measurements. No evidence was found for the presence of C—IV, $CO^3_{2,}$ at approximately 289 eV. The N 1s exhibited a single peak at 399.0 eV, which was attributed to sp. 3 and sp. 2, C—N and C—NH_2 bondings, respectively (Kim et al., 2012).

3.2. Nanobiochar–adsorbate interaction studies

3.2.1. Effect of pH on adsorption behaviour

The pattern of adsorption at different pH levels was investigated to identify the highest adsorbed pH value since the pH of the media determines the surface complexation of OTC and GL on NBC. The edge experiment demonstrated maximum adsorptions of 15 mg/g OTC and 16.58 mg/g GL at pH 6 and 7, respectively (Fig. 4a and b). Both OTC and GL depict speciation with fluctuations in solution pH, as mentioned in the literature (Mamindy-Pajany et al., 2014). The point of zero charge (pHzpc) of dendro biochar was observed at pH 7.4 (Wathukarage et al., 2017), which clearly explains the role of OTC and GL adsorption. Therefore, according to the pHzpc data obtained during the edge experiment, the NBC surface remains positively charged until the solution reaches a pH of 7.4, and after passing the pHzpc it is negatively charged.

Simultaneously, the protonation or deprotonation of ionisable functional groups of OTC and GL molecules can occur depending on the pH of the media (Fig. 4a and b). At pH < 3.5, the cationic form of OTC is dominant, while the zwitterionic form prevails in the pH range of 3.5–7.5 and the anionic form is dominant at pH > 7.5. Considering GL, the cationic form is predominant at pH below 2, while the zwitterionic form is dominant at pH 1–2 and the anionic form is predominant at pH

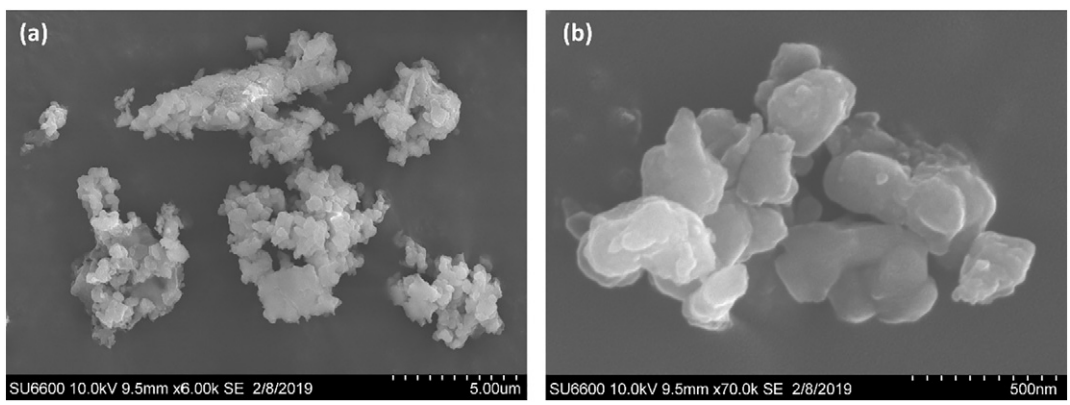

Fig. 2. SEM images of polygonal-shaped nanobiochar particles and occasional agglomeration at a magnification of (a) ×6 k and (b) ×70 k.

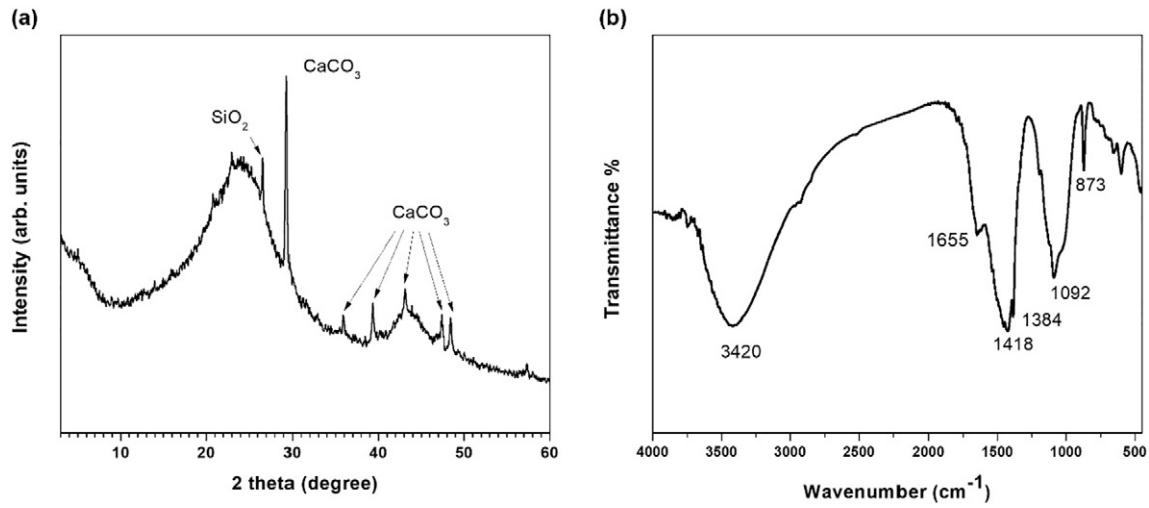

Fig. 3. (a) PXRD pattern and (b) FTIR spectrum of pristine nanobiochar.

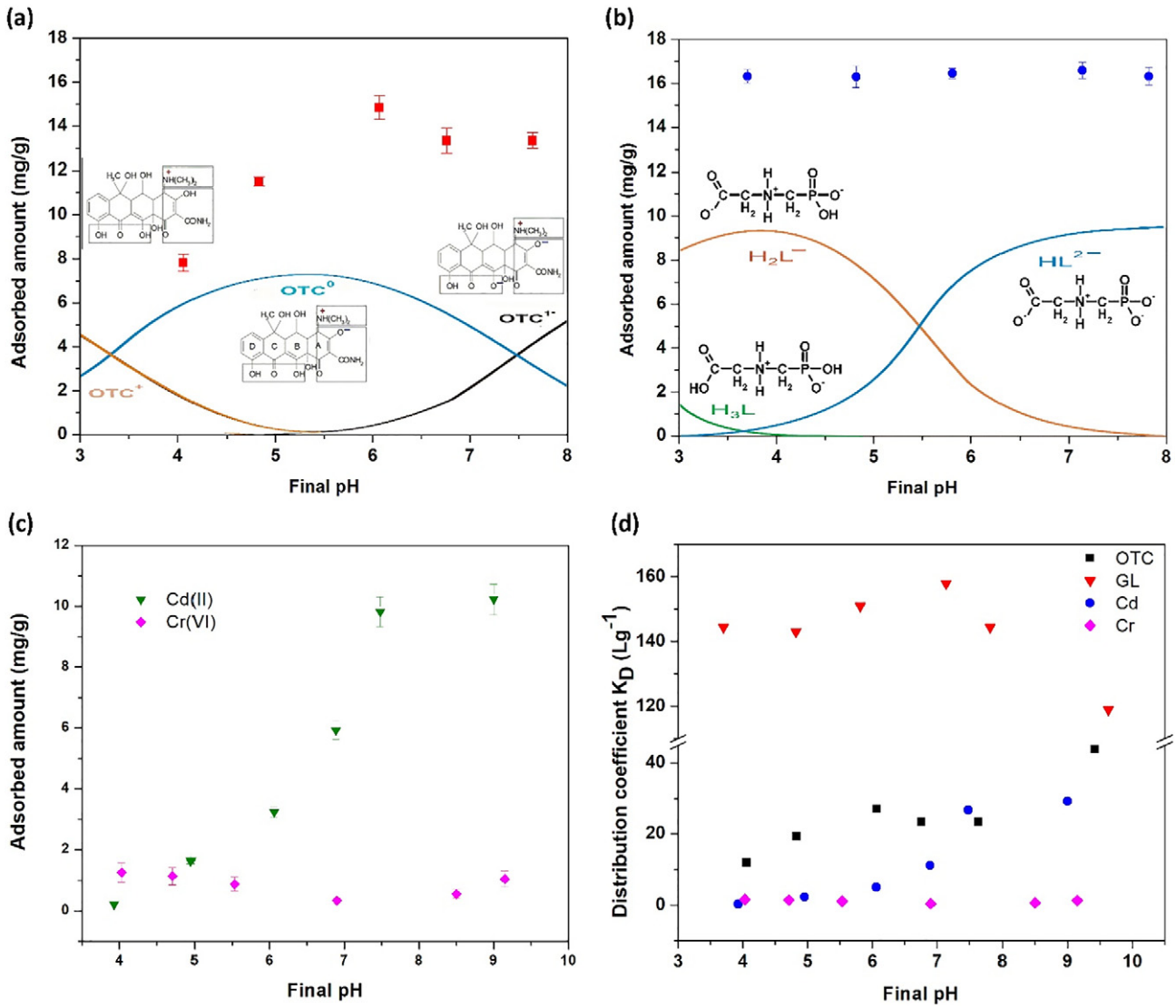

Fig. 4. Adsorption edges (a) and (b) speciation of OTC and GL, cationic, zwitterion, and anionic forms, with the final pH at initial OTC and GL concentrations of 25 and 20 mg/L, respectively. (c) Effect of pH with the adsorbed amount of Cd(II) and Cr(VI) at initial concentrations of 10 and 5 mg/L, respectively. (d) Distribution coefficients (K_D) for OTC, GL, Cd(II), and Cr(VI)-loaded NBC in the pH range of 3–10.

above 2. Consequently, in the experimental pH range, zwitterionic and anionic forms exist.

Taking into account the pHzpc, above pH 7.4 positively charged dimethylamine group of OTC zwitterion (Fig. 4a) and positively charged amide group (—NH_2^+) of GL zwitterion (Fig. 4b), form complexes with the deprotonated NBC surface. Therefore, the interaction of OTC and GL with NBC can be suggested as a physisorption process through electrostatic and van der Waals attractions.

The structure of NBC contains surface functional groups, such as phenolic —OH, aldehyde/ketone C═O, and Si—O, which can be negatively charged at experimental pHs from 3 to 7 (Goyne et al., 2002). This suggests covalent or coordination binding of the positive end of the zwitterionic form of OTC (pH 3.5–7.5) to NBC surface functional groups as plausible chemisorptive mechanisms. On the other hand, since zwitterionic and cationic forms of GL (pH 1–2) are not present in the experimental pH range, the possibility of chemisorptive binding of GL to NBC can be rejected.

In the case of Cd and Cr, the edge experiment revealed maximum adsorptions of 10 and 1.2 mg/g at pH 9 and 4, respectively (Fig. 4a and b). Cadmium exists as a cation (Cd^{2+}) in aqueous media and has the ability to bind to the negatively charged NBC surface at pH above 7.4 (pHzpc) in a non-specific manner. Negatively charged dichromate ions ($Cr_2O_7^{2-}$) are repelled from the negatively charged NBC surface, confirming that the physisorption mechanism does not occur in the binding of Cr to NBC. Positively charged calcium (Ca^{2+}) ions on the NBC surface provide binding sites to $Cr_2O_7^{2-}$ ions due to electrostatic attraction, which is adsorption-specific. Dichromate ions can be reduced to Cr^{3+} ions and demonstrate surface complexation with NBC functional groups, such as aldehyde/ketone C═O and —OH.

3.2.2. Distribution coefficient data

Solution pH and chemical speciation values of the OTC, GL, Cd(II), and Cr(VI) molecules depend strongly on the distribution coefficient (K_D), which is the ratio of the maximum adsorption capacity to the equilibrium concentration (ECETOC, 2014). When the K_D value is higher than 100 L/g, it confirms that the adsorbate is well bonded to the surface. However, it does not indicate sorption strength. For GL, a minor increase in K_D values was observed up to pH 7, and a maximum K_D value of 158 L/g was achieved (Fig. 4d). Above pH 7, a rapid decrease in K_D was observed up to pH 9.6. The other adsorbates, i.e., Cd(II), OTC, and Cr(VI), did not have K_D values higher than 100 L/g. However, increasing K_D values can be seen in both OTC and Cd(II) up to pH 9.5 while Cr(VI) did not demonstrate any increase or higher K_D value, which may be attributed to its negative surface.

3.2.3. Effect of different adsorbate loading

The relationship between the adsorbed amount (OTC, GL, Cd, and Cr) and the solution concentration at equilibrium is described by adsorption isotherm studies (Fig. 4a–d). Among the four different adsorbates, GL and Cr(VI) reached equilibrium at experimental concentrations. For GL, the maximum experimental adsorption capacity (Q_{max}) was 83 mg/g at an equilibrium concentration of 17 mg/L, whereas the Q_{max} for Cr(VI) was 7.4 mg/g at an equilibrium concentration of 66 mg/L.

3.2.4. Data modelling

It has been assumed that the shape of the isotherm curve indicates the adsorption mechanism based on experimental concentrations. In order to comprehend the adsorption mechanism, isotherm data were modelled by the Hills, Freundlich, Langmuir, Temkin, and Redlich–Peterson equations. The Hills equation offered the best fit for the four adsorbates. The Freundlich equation also showed a decent fit for OTC and Cd(II). The Hills model revealed the best fit ($R^2 = 0.993$) for OTC, while the Freundlich model showed a partial fit ($R^2 = 0.98$; Table 1). The trend of increasing adsorbed amount did not reach the equilibrium concentration even after 350 mg/L and exhibited a maximum adsorption capacity of 520 mg/g. The metal ion Cd(II) showed a similar trend

Table 1
Isotherm model parameters for the adsorption of OTC, GL, Cd(II), and Cr(VI) on nanobiochar at 0.5 g/L loading.

Experimentation	Model	Parameter	Value
Isotherm models for OTC	Hill	K_D	0.004
	$q_{ads} = \frac{q_{sn}C_e^{n_H}}{K_D + C_e^{n_H}}$	n_H	2.9536
		Q_{max} (mg/g)	519.95
		R^2	0.993
		Chi^2	145.29
	Freundlich	K_f (mg/g)/(mg/L)^n	0.039
	$q_e = K_f C_e^n$	n	1.606
		R^2	0.980
		Chi^2	362.99
Isotherm models for GL	Hill	K_D	0.167
		n_H	3.39
		Q_{max} (mg/g)	81.87
		R^2	0.982
		Chi^2	30.07
Isotherm models for Cd(II)	Hill	K_D	0.007
		n_H	2.42
		Q_{max} (mg/g)	922.27
		R^2	0.997
		Chi^2	171.33
	Freundlich	K_f (mg/g)/(mg/L)^n	0.45
		n	1.41
		R^2	0.98
		Chi^2	1005.1
Isotherm models for Cr(VI)	Hill	K_D	0.05
		n_H	3.90
		Q_{max} (mg/g)	7.46
		R^2	0.968
		Chi^2	0.36

to that of OTC, with the best fit for the Hills model ($R^2 = 0.997$) and a decent fit for the Freundlich model ($R^2 = 0.98$). An extremely high maximum adsorption capacity of 922 mg/g was observed, confirming the excellent removal possibility of cations with negatively charged surfaces, such as biochar. Both GL and Cr(VI) fit only to the Hills model, with maximum adsorption capacities of 82 and 7.46 mg/g and R^2 values of 0.982 and 0.968, respectively (Fig. 5).

Among the many different types of isotherms, the S-type isotherm curve represents a complex situation, which may be due to interactions between the surface and the previously sorbed molecules until the binding effect drops with the affinity. Cooperative adsorption occurs in the initial part of the S-curve, which implies a side-by-side association between the adsorbent surface and adsorbate molecules (Giles et al., 1960). The Hill isotherm model is a three-parameter model that theorises the cooperative phenomenon of different binding species on homogenous substrates. The ligand-binding ability at one site on an adsorbent molecule influences different binding sites on the same adsorbent macromolecule (Farouq and Yousef, 2015). Possible binding mechanisms are considered as: $nH > 1$, positive cooperative binding; $nH = 1$, noncooperative or hyperbolic binding; and $nH < 1$, negative cooperative binding (Saadi et al., 2015). The four types of adsorbates exhibit $nH > 1$, confirming that positive cooperative binding occurred between the adsorbate molecules and NBC. The positive cooperative binding is attributed to the influence of a previously bound adsorbate at the NBC binding site, which increased the affinity towards another binding site (Cattoni et al., 2015). In the isotherm curve, a high affinity (k_f) is indicated by a high initial isotherm slope and a high sorptive index, with the Hills model exhibiting a closer behaviour compared to the Freundlich model (Saadi et al., 2015).

The Freundlich model hypothesises that the adsorbent surface is heterogeneous and that the active sites and their energies are distributed exponentially (Garcıa et al., 2004). The previously occupied binding sites are comparatively stronger until the energy decreases exponentially with the completion of the adsorption process. This particular model assumes multilayer adsorption and can be applied as another form of the Langmuir model, which can also be applied to multilayer adsorption (Garcıa et al., 2004). In the Freundlich isotherm,

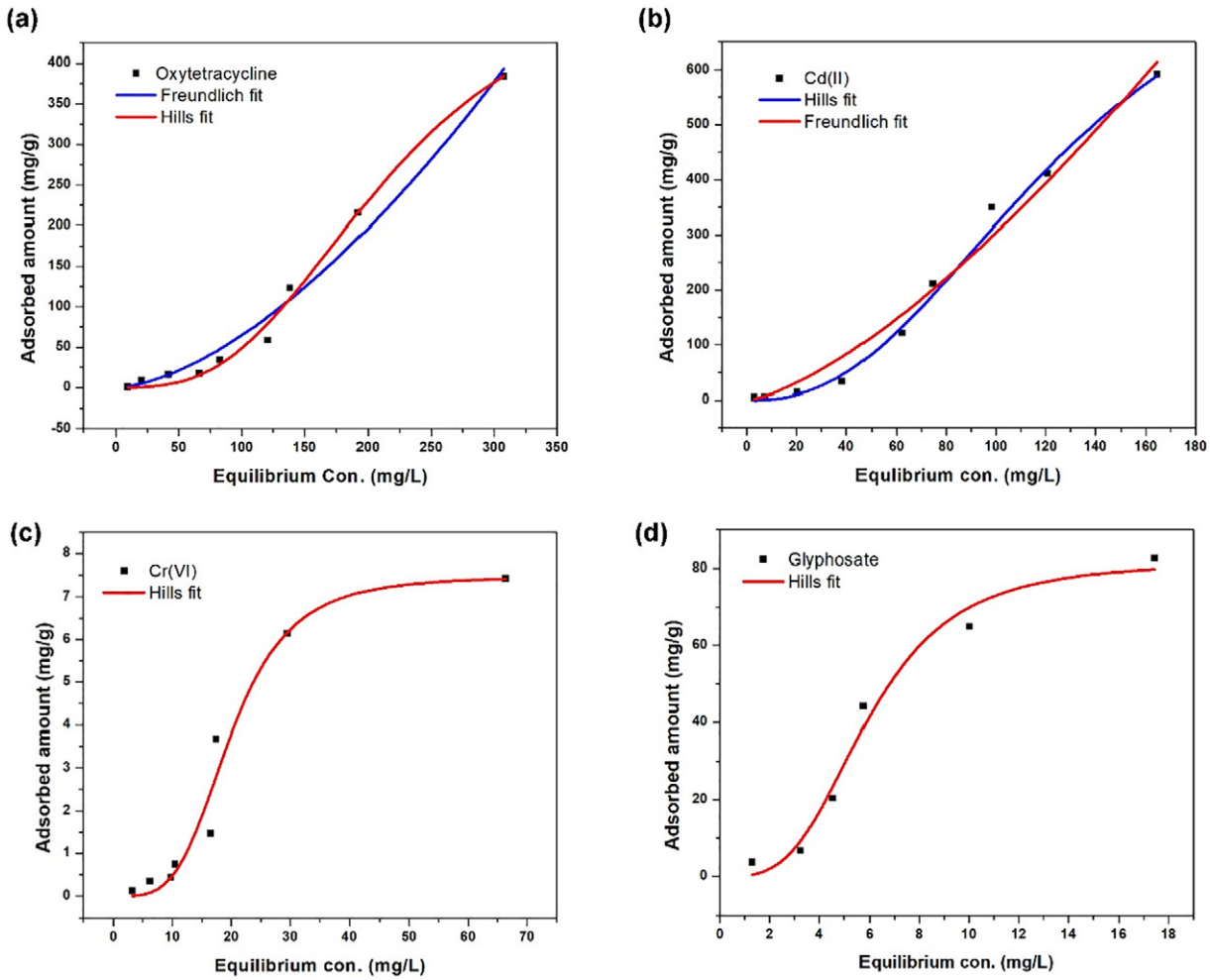

Fig. 5. Experimental data on initial adsorbate concentrations vs. adsorbed amounts in the pH range of 4–10 and at NBC dosage of 0.5 g/L. Symbols represent experimental data, whereas lines indicate modelled data using the nonlinear least-squares fit of Hills and Freundlich equations.

n indicates the adsorption strength of the contaminant on the adsorbent or the heterogeneity of the sorbent surface. Therefore, $n > 1$ indicates favourable adsorption of the contaminant on the adsorbent surface. In this study, the Freundlich model was decently fitted to OTC and Cd(II) with $n > 1$, indicating a favourable binding of OTC and Cd(II) to NBC. A higher value of n reflects a higher intensity of adsorption. When the value of n is low and close to zero, the heterogeneity increases and the adsorption isotherm becomes increasingly nonlinear. However, it was not observed in this study (Rao et al., 2009). Furthermore, $1/n < 0.1$ denotes irreversible sorption. The experimental data modelling for OTC and Cd(II) resulted in 1/n values of 0.62 and 0.71, respectively, indicating that the adsorption mechanism is reversible. Therefore, the recovery of NBC may be possible by desorption.

The capacity of adsorbents determines the prospective removal of contaminants from aqueous media. However, the comparison between different adsorbents with adsorption capacities was unsuccessful due to factors such as the initial concentration of adsorbate, etc. Therefore, to better understand the different sorption capabilities, PC was introduced. A fair comparison between materials can be carried out with the PC, which represents the ratio between the sorbed adsorbate and equilibrium concentration of adsorbate (Vikrant and Kim, 2018). The performance of a particular adsorbent can be determined and compared with other adsorbents using the PC. The PC can be obtained by dividing the maximum adsorption capacity (mg/g) of the adsorbent by the equilibrium concentration (mg/L) of the adsorbate (Vikrant and Kim, 2018). Table 2 shows the comparison of different biochar types with calculated PCs. From the table, it is evident that NBC exhibits the highest PC among the four adsorbates, which means that it possesses the highest adsorption capacity compared with other types of biochar.

3.2.5. Influence of surface functional groups for adsorption

The FTIR spectrums of OTC, GL, Cr(VI), and Cd(II) loaded NBC show significant differences in some of the peak intensities and peak shifts compared with the FTIR spectrum of pristine NBC. Regarding organic adsorbate OTC, skeletal C═C (aromatic ring) vibrations and —CH_2 medium-to-strong peaks exhibited at approximately 1430 and 2925 cm^{-1}, respectively (Punamiya et al., 2013). The shoulder at 1645 cm^{-1} confirms the C═O group of amides (—$CONH_2$), while the sharp peak around 872 cm^{-1} suggests aromatic rings (Punamiya et al., 2013). In GL, the peak obtained around 1194 cm^{-1} is attributed to the P═O bond, with the two single bonds between the phosphorus atom and two oxygen atoms that depict the asymmetric and symmetric vibrations around 1087 and 1194 cm^{-1}. Regarding the two inorganic metal ions that have been studied, Cd(II) exhibits two peaks at around 1092 cm^{-1} and 1643 cm^{-1}, while Cr(VI) depicts three peaks at 654 cm^{-1}, 953 cm^{-1}, and 1418 cm^{-1} (Osasona et al., 2018). The peak at 1384 cm^{-1} showed a sharp increment in intensity after the adsorption of Cd(II) (Fig. 6).

3.2.6. XPS investigations

The optimum deconvolution of N 1s after OTC adsorption demonstrated two peaks at 399.5 eV and 402.3 eV, which were attributed to —NH— or —NH_2 and C—N—C (Chen et al., 2019). After adsorption of OTC, the C 1s bands shifted upward owing to the protonated amines

Table 2
Comparison of different types of biochar, including NBC and their highest removal capacities for GL, OTC, Cd(II), and Cr(VI).

Adsorbent	Carbon type	Feedstock	Temperature °C	Q_{max} (mg/g)	PC value Lg^{-1}	pH	Ref
Glyphosate	Woody biochar	Dendro	700–1000	44	0.73	5	(Mayakaduwa et al., 2016)
	Activated carbon	Coconut shell		0.0173	0.06	8	(Dissanayake Herath et al., 2019)
	Rice husk biochar	Rice husk	700	123.03	2.3	4	(Herath et al., 2016)
	Woody biochar	Apple wood	700	0.07	0.06	8	(Hall et al., 2018)
	Nanobiochar	Dendro	700	83	4.76	7	Present study
Oxytetracycline	Activated woody biochar (5 M H_3PO_4)	Wood residues	600	254.1	4.74	4	(Aghababaei et al., 2017)
	Activated woody biochar (5 M H_3PO_4)	Forest residue	600	263.8	5.36	4	(Aghababaei et al., 2017)
	Magnetised biochar composite	Natural attapulgite, cauliflower leaves	300	35.2	0.42	4.5	(Wang et al., 2019)
	Modified cassava waste biochar (KOH)	Cassava waste	500	10	0.12	9	(Luo et al., 2018)
	Nanobiochar	Dendro	700	520	44	9	Present study
Cd(II)	Activated woody biochar (1 M KOH)	Wood residues	600	72	0.44	6	(Aghababaei et al., 2017)
	Activated woody biochar (1 M NaOH)	Forest residues	600	79.3	0.53	6	(Aghababaei et al., 2017)
	Wheat straw biochar (WSBC)	Wheat straw	700	69.8	0.6	5	(Liu and Fan, 2018)
	Buffalo weed biochar	Buffalo weed	700	25.8	2.6	3–6	(Li et al., 2016)
	Nanobiochar	Dendro	700	922	29	9	Present study
Cr(VI)	Sugar beet tailing biochar	Sugar beet tailing	300	123	0.2	2	(Dong et al., 2011)
	Magnetised peanut hull biochar	Peanut hull	650	78	0.37	5	(Han et al., 2016)
	Artemisia argyi stem derived biochar	*Artemisia argyi* stem	600	162	0.22	1–4	(Song et al., 2019)
	Nanobiochar	Dendro	700	7.46	1.6	4	Present study

or the formation of hydrogen bonds (Liu et al., 2012). Both C 1s and N 1s indicated a high binding intensity after adsorption. The visible peak changed from 83.9 to 284.9 eV and from 285.5 to 286.8 eV, indicating the interaction of C—C and (C—II) C—O, and C—H and C—N, respectively (Fig. 7). Furthermore, the formation of a new peak at N 1s 402.4 eV similar to Cr(VI), demonstrates the involvement of amino groups in NBC in the OTC-NBC interaction (Fig. 7).

In the case of GL, the O 1s peaks for C—O or H—O—C at 531.9 eV demonstrated a redshift to 530.9 eV, indicating the involvement of O-containing groups (Supplementary materials). The involvement of C—C and (C—II) C—O, C—H, and C—N was observed by the peak changes in C 1s. The XPS spectra of the N 1s peak presents a triplet peak centred at 399.2, 400.4, and 401.9 eV, indicating the presence of protonated and nonprotonated nitrogen, respectively (Flores et al., 2018).

The optimum deconvolution peak fitting for the Cr 2p region obtained a plausible assignment of four peaks, which implies the presence of Cr(III) after adsorption of Cr(VI) on NBC. According to the literature, this is attributed to the reduction of Cr(VI) by functional groups (Chen et al., 2018). Adsorption of Cr(VI) on NBC demonstrates the loss of peak intensity, and a slight blue shift in the O 1s region denotes the involvement of O-bearing functional groups in hexavalent Cr removal. The bands at 576–578 and 586–589 eV are attributed to Cr 2p 3/2 and Cr 2p 1/2, respectively (He et al., 2019). The presence of Cr(VI) is denoted by the peaks at 578.7 and 587.9 eV, while the small bands at 576.3 and 581.2 eV correspond to the presence of Cr(III) due to the partial/incomplete reduction by NBC surface functional groups (Chen et al., 2018). Reduced adsorption of Cr(VI) in the experimental data is consistent with the XPS observations. Relative peak areas of oxygen-containing functional groups on the NBC surface, such as hydroxyl, carboxyl, and carbonyl decreased, indicating their involvement in providing electrons for the reduction of Cr(VI). Furthermore, C—C (284.0 eV), C—O (285.5 eV), and C═O (287.1 eV) bands demonstrated blue shifts, and C—Cr or C═O[$Cr(CO)_6$] bond formation was observed at 287.5 eV in the Cr(VI) treated NBC (Chen et al., 2018). The minor shift of the C—N or C═N and new peak formation at 399.3 eV indicate the involvement of amino groups in the Cr interaction.

The types of coordination bonding between Cd(II) and NBC functional groups were identified in the XPS spectra of C 1s, O 1s, and N 1s, as shown in Fig. 6. The adsorption of Cd(II) on NBC showed an

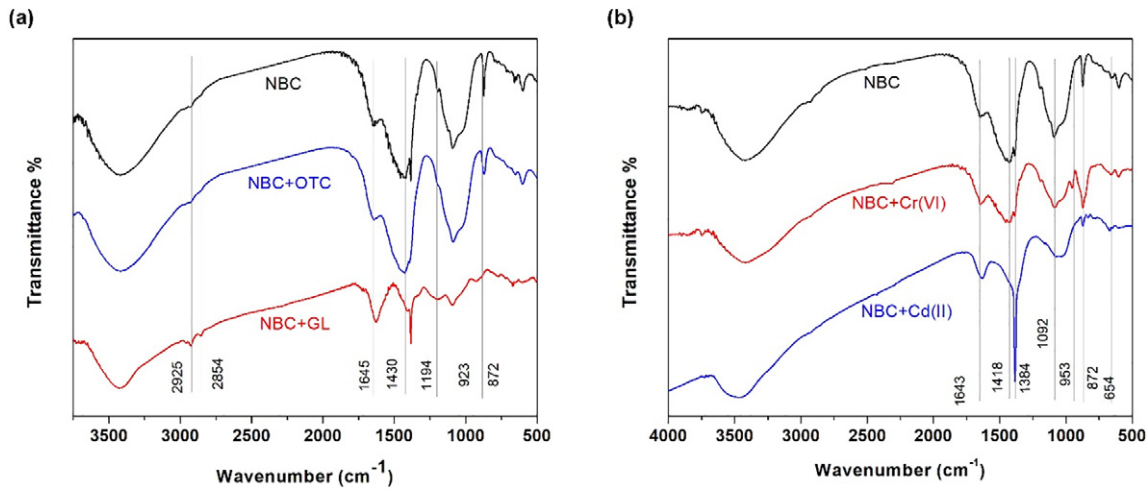

Fig. 6. Comparison of FTIR patterns for (a) OTC and GL (organic contaminants), and (b) Cr(VI) and Cd(II) loaded NBC with pristine NBC.

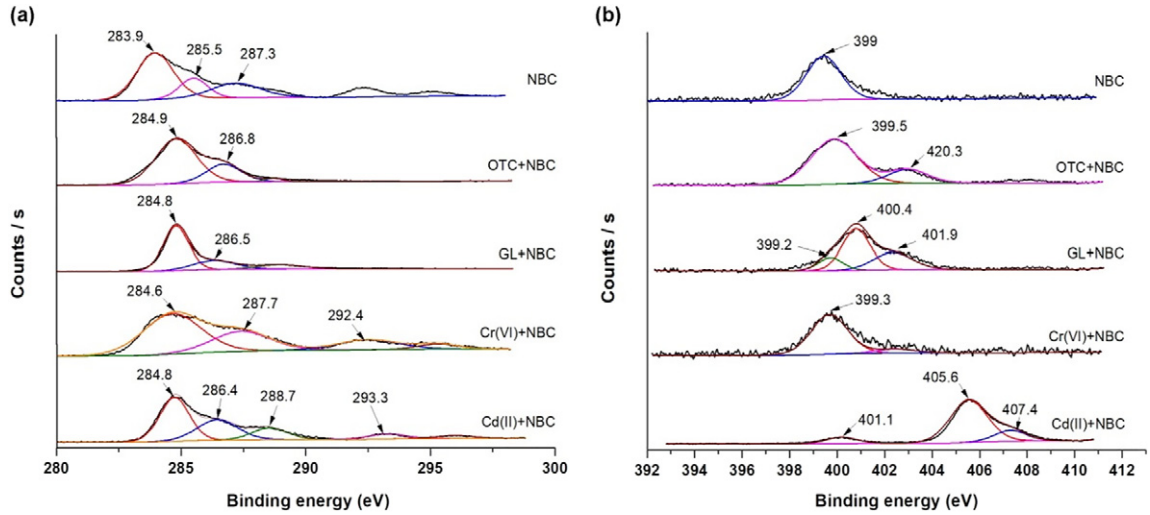

Fig. 7. XPS scanning spectra of pristine NBC and OTC, GL, Cr(VI), and Cd(II) loaded NBC. XPS high-resolution survey scans of (a) C 1s and (b) N 1s region of pristine and contaminant-loaded NBC.

apparent increase in C 1s peaks. Oxygen-bearing functional groups, such as phenolic and carboxylic in NBC, are responsible for Cd(II) adsorption, which is indicated by the increase in binding energy (Bian et al., 2015). All C—I, C—II, and C—III showed an increased binding energy after Cd (II) interaction with NBC. The slight blue shifts, from 530.8 to 532.5 eV in O—I and from 285.5 to 286.4 eV in C—II, were attributed to the involvement of phenolic groups in Cd adsorption by NBC, indicating that the O atom donated its electron density to the Cd ion during adsorption (Liu et al., 2013). The case of C—N and C—NH_2 involvement in Cd adsorption is shown by the slight blue shift from 399 to 401 eV. The broad peak at 405 eV is due to the nitrate from the Cd salt added during the adsorption experiment.

4. Conclusions

The present study applied a facile synthesis process for the preparation of NBC from the waste product of a thermal power plant. The resulting NBC has a graphitic nature, as evidenced by the results of SEM, BET, and XPS. The successful removal of OTC, GL, Cr(VI), and Cd (II) from aqueous media was exhibited with high adsorption capacities of 520, 83, 7.46, and 922 mg/g, respectively. Although the adsorption capacities achieved are moderately lower compared with data reported in the literature, the adsorption performance, represented by the PC, demonstrated higher values for NBC. The Hills equation was noticeably fitted to OTC, GL, Cd, and Cr(VI) values, indicating the cooperativity of multiple binding sites for NBC. From the Hills cooperativity coefficient values (nH), a positive cooperative binding mechanism between the adsorbate molecules and NBC was identified for the four types of adsorbates. This study demonstrated that the structural breakdown of biochar through disc milling yields nanobiochar of graphitic nature with an elevated adsorption performance.

Supplementary data to this article can be found online at https://doi.org/10.1016/j.scitotenv.2019.135725.

Declaration of competing interest

We hereby inform you that there is no conflict of interest among authors.

Acknowledgements

The authors appreciate the support of the Instrument Center, Faculty of Applied Sciences, University of Sri Jayewardenepura, Sri Lanka.

References

Agency, E.M., 2017. Sales of veterinary antimicrobial agents in 30 European countries in 2015. Trends From 2010 to 2015.
Aghababaei, A., Ncibi, M.C., Sillanpää, M., 2017. Optimized removal of oxytetracycline and cadmium from contaminated waters using chemically-activated and pyrolyzed biochars from forest and wood-processing residues. Bioresour. Technol. 239, 28–36. https://doi.org/10.1016/j.biortech.2017.04.119.
Asfaw, T.B., Tadesse, T.M., Ewnetie, A.M., 2017. Determination of total chromium and chromium species in Kombolcha tannery wastewater, surrounding soil, and lettuce plant samples, South Wollo, Ethiopia. Adv. Chem. 2017.
Ashiq, A., Adassooriya, N.M., Sarkar, B., Rajapaksha, A.U., Ok, Y.S., Vithanage, M., 2019. Municipal solid waste biochar-bentonite composite for the removal of antibiotic ciprofloxacin from aqueous media. J. Environ. Manag. 236, 428–435.
Bayram, M., Öner, M.D., 2007. Bulgur milling using roller, double disc and vertical disc mills. J. Food Eng. 79, 181–187. https://doi.org/10.1016/j.jfoodeng.2006.01.042.
Bian, Y., Bian, Z., Zhang, J., Ding, A., Liu, S., Zheng, L., Wang, H., 2015. Adsorption of cadmium ions from aqueous solutions by activated carbon with oxygen-containing functional groups. Chinese J. Chem. Eng. 23, 1705–1711. https://doi.org/10.1016/j.cjche.2015.08.031.
Cattoni, D.I., Chara, O., Kaufman, S.B., González Flecha, F.L., 2015. Cooperativity in binding processes: new insights from phenomenological modeling. PLoS One 10, e0146043. https://doi.org/10.1371/journal.pone.0146043.
Chen, Y., An, D., Sun, S., Gao, J., Qian, L., 2018. Reduction and removal of chromium VI in water by powdered activated carbon. Mater. (Basel, Switzerland) 11, 269. https://doi.org/10.3390/ma11020269.
Chen, Y., Shi, J., Du, Q., Zhang, H., Cui, Y., 2019. Antibiotic removal by agricultural waste biochars with different forms of iron oxide. RSC Adv. 9, 14143–14153.
Daghrir, R., Drogui, P., 2013. Tetracycline antibiotics in the environment: a review. Environ. Chem. Lett. 11, 209–227.
Dissanayake Herath, G.A., Poh, L.S., Ng, W.J., 2019. Statistical optimization of glyphosate adsorption by biochar and activated carbon with response surface methodology. Chemosphere 227, 533–540. https://doi.org/10.1016/j.chemosphere.2019.04.078.
Dong, X., Ma, L.Q., Li, Y., 2011. Characteristics and mechanisms of hexavalent chromium removal by biochar from sugar beet tailing. J. Hazard. Mater. 190, 909–915. https://doi.org/10.1016/j.jhazmat.2011.04.008.
ECETOC, 2014. Environmental Risk Assesment of Ionisable Compounds.
Fan, X., Chang, D.W., Chen, X., Baek, J.-B., Dai, L., 2016. Functionalized graphene nanoplatelets from ball milling for energy applications. Curr. Opin. Chem. Eng. 11, 52–58.
Farouq, R., Yousef, N.S., 2015. Equilibrium and kinetics studies of adsorption of copper (II) ions on natural biosorbent. Int. J. Chem. Eng. Appl. 6, 319.
Flores, F.M., Sánchez, R.M.T., dos Santos Afonso, M., 2018. Some aspects of the adsorption of glyphosate and its degradation products on montmorillonite. Environ. Sci. Pollut. Res. 25, 18138–18146.
Garcıa, G., Faz, A., Cunha, M., 2004. Performance of *Piptatherum miliaceum* (Smilo grass) in edaphic Pb and Zn phytoremediation over a short growth period. Int. Biodeterior. Biodegradation 54, 245–250.
Giles, C.H., MacEwan, T.H., Nakhwa, S.N., Smith, D., 1960. 786. Studies in adsorption. Part XI. A system of classification of solution adsorption isotherms, and its use in diagnosis of adsorption mechanisms and in measurement of specific surface areas of solids. J. Chem. Soc., 3973–3993 https://doi.org/10.1039/JR9600003973.
Goyne, K.W., Zimmerman, A.R., Newalkar, B.L., Komarneni, S., Brantley, S.L., Chorover, J., 2002. Surface charge of variable porosity Al_2O_3(s) and SiO_2(s) adsorbents. J. Porous. Mater. 9, 243–256. https://doi.org/10.1023/A:1021631827398.
Hall, K.E., Spokas, K.A., Gamiz, B., Cox, L., Papiernik, S.K., Koskinen, W.C., 2018. Glyphosate sorption/desorption on biochars–interactions of physical and chemical processes. Pest Manag. Sci. 74, 1206–1212.

Han, Y., Cao, X., Ouyang, X., Sohi, S.P., Chen, J., 2016. Adsorption kinetics of magnetic biochar derived from peanut hull on removal of Cr (VI) from aqueous solution: effects of production conditions and particle size. Chemosphere 145, 336–341. https://doi.org/10.1016/j.chemosphere.2015.11.050.

He, R., Yuan, X., Huang, Z., Wang, H., Jiang, L., Huang, J., Tan, M., Li, H., 2019. Activated biochar with iron-loading and its application in removing Cr (VI) from aqueous solution. Colloids Surfaces A Physicochem. Eng. Asp. 579, 123642. https://doi.org/10.1016/j.colsurfa.2019.123642.

Herath, I., Kumarathilaka, P., Navaratne, A., Rajakaruna, N., Vithanage, M., 2015. Immobilization and phytotoxicity reduction of heavy metals in serpentine soil using biochar. J. Soils Sediments 15, 126–138.

Herath, I., Kumarathilaka, P., Al-Wabel, M.I., Abduljabbar, A., Ahmad, M., Usman, A.R.A., Vithanage, M., 2016. Mechanistic modeling of glyphosate interaction with rice husk derived engineered biochar. Microporous Mesoporous Mater. 225, 280–288. https://doi.org/10.1016/j.micromeso.2016.01.017.

Karinkanta, P., Ämmälä, A., Illikainen, M., Niinimäki, J., 2018. Fine grinding of wood – overview from wood breakage to applications. Biomass Bioenergy 113, 31–44. https://doi.org/10.1016/j.biombioe.2018.03.007.

Kim, H.J., Bae, I.-S., Cho, S.-J., Boo, J.-H., Lee, B.-C., Heo, J., Chung, I., Hong, B., 2012. Synthesis and characteristics of NH2-functionalized polymer films to align and immobilize DNA molecules. Nanoscale Res. Lett. 7, 30. https://doi.org/10.1186/1556-276X-7-30.

Li, F., Shen, K., Long, X., Wen, J., Xie, X., Zeng, X., Liang, Y., Wei, Y., Lin, Z., Huang, W., 2016. Preparation and characterization of biochars from Eichornia crassipes for cadmium removal in aqueous solutions. PLoS One 11, e0148132.

Lian, F., Yu, W., Wang, Z., Xing, B., 2018. New insights into black carbon nanoparticle-induced dispersibility of goethite colloids and configuration-dependent sorption for phenanthrene. Environ. Sci. Technol. 53, 661–670.

Liu, L., Fan, S., 2018. Removal of cadmium in aqueous solution using wheat straw biochar: effect of minerals and mechanism. Environ. Sci. Pollut. Res. 25, 8688–8700. https://doi.org/10.1007/s11356-017-1189-2.

Liu, P., Liu, W.-J., Jiang, H., Chen, J.-J., Li, W.-W., Yu, H.-Q., 2012. Modification of bio-char derived from fast pyrolysis of biomass and its application in removal of tetracycline from aqueous solution. Bioresour. Technol. 121, 235–240. https://doi.org/10.1016/j.biortech.2012.06.085.

Liu, H., Gao, Q., Dai, P., Zhang, J., Zhang, C., Bao, N., 2013. Preparation and characterization of activated carbon from lotus stalk with guanidine phosphate activation: sorption of Cd(II). J. Anal. Appl. Pyrolysis 102, 7–15. https://doi.org/10.1016/j.jaap.2013.04.010.

Luo, J., Li, X., Ge, C., Müller, K., Yu, H., Huang, P., Li, J., Tsang, D.C.W., Bolan, N.S., Rinklebe, J., Wang, H., 2018. Sorption of norfloxacin, sulfamerazine and oxytetracycline by KOH-modified biochar under single and ternary systems. Bioresour. Technol. 263, 385–392. https://doi.org/10.1016/j.biortech.2018.05.022.

Lyu, H., Gao, B., He, F., Zimmerman, A.R., Ding, C., Huang, H., Tang, J., 2018. Effects of ball milling on the physicochemical and sorptive properties of biochar: experimental observations and governing mechanisms. Environ. Pollut. 233, 54–63. https://doi.org/10.1016/j.envpol.2017.10.037.

Mamindy-Pajany, Y., Sayen, S., Mosselmans, J.F.W., Guillon, E., 2014. Copper, nickel and zinc speciation in a biosolid-amended soil: pH adsorption edge, μ-XRF and μ-XANES investigations. Environ. Sci. Technol. 48, 7237–7244.

Mayakaduwa, S.S., Kumarathilaka, P., Herath, I., Ahmad, M., Al-Wabel, M., Ok, Y.S., Usman, A., Abduljabbar, A., Vithanage, M., 2016. Equilibrium and kinetic mechanisms of woody biochar on aqueous glyphosate removal. Chemosphere 144, 2516–2521.

Mohan, D., Sarswat, A., Ok, Y.S., Pittman Jr., C.U., 2014. Organic and inorganic contaminants removal from water with biochar, a renewable, low cost and sustainable adsorbent–a critical review. Bioresour. Technol. 160, 191–202.

Naghdi, M., Taheran, M., Brar, S.K., Rouissi, T., Verma, M., Surampalli, R.Y., Valero, J.R., 2017a. A green method for production of nanobiochar by ball milling-optimization and characterization. J. Clean. Prod. 164, 1394–1405. https://doi.org/10.1016/j.jclepro.2017.07.084.

Naghdi, M., Taheran, M., Pulicharla, R., Rouissi, T., Brar, S.K., Verma, M., Surampalli, R.Y., 2017b. Pine-wood derived nanobiochar for removal of carbamazepine from aqueous media: adsorption behavior and influential parameters. Arab. J. Chem. https://doi.org/10.1016/j.arabjc.2016.12.025 (In press).

Naghdi, M., Taheran, M., Brar, S.K., Kermanshahi-pour, A., Verma, M., Surampalli, R.Y., 2019. Fabrication of nanobiocatalyst using encapsulated laccase onto chitosan-nanobiochar composite. Int. J. Biol. Macromol. 124, 530–536. https://doi.org/10.1016/j.ijbiomac.2018.11.234.

Nath, B.K., Chaliha, C., Kalita, E., 2019. Iron oxide permeated mesoporous rice-husk nanobiochar (IPMN) mediated removal of dissolved arsenic (As): chemometric modelling and adsorption dynamics. J. Environ. Manag. 246, 397–409. https://doi.org/10.1016/j.jenvman.2019.06.008.

Osasona, I., Aiyedatiwa, K., Johnson, J., Faboya, O.L., 2018. Activated carbon from spent brewery barley husks for cadmium ion adsorption from aqueous solution. Indones. J. Chem. 18, 145–152.

Peterson, S.C., Jackson, M.A., Kim, S., Palmquist, D.E., 2012. Increasing biochar surface area: optimization of ball milling parameters. Powder Technol. 228, 115–120. https://doi.org/10.1016/j.powtec.2012.05.005.

Punamiya, P., Sarkar, D., Rakshit, S., Datta, R., 2013. Effectiveness of aluminum-based drinking water treatment residuals as a novel sorbent to remove tetracyclines from aqueous medium. J. Environ. Qual. 42, 1449–1459.

Rajapaksha, A.U., Chen, S.S., Tsang, D.C.W., Zhang, M., Vithanage, M., Mandal, S., Gao, B., Bolan, N.S., Ok, Y.S., 2016. Engineered/designer biochar for contaminant removal/immobilization from soil and water: potential and implication of biochar modification. Chemosphere https://doi.org/10.1016/j.chemosphere.2016.01.043.

Rajapaksha, A.U., Alam, M.S., Chen, N., Alessi, D.S., Igalavithana, A.D., Tsang, D.C.W., Ok, Y.S., 2018. Removal of hexavalent chromium in aqueous solutions using biochar: chemical and spectroscopic investigations. Sci. Total Environ. 625, 1567–1573. https://doi.org/10.1016/j.scitotenv.2017.12.195.

Rao, M.M., Ramana, D.K., Seshaiah, K., Wang, M.C., Chien, S.W.C., 2009. Removal of some metal ions by activated carbon prepared from *Phaseolus aureus* hulls. J. Hazard. Mater. 166, 1006–1013.

Saadi, R., Saadi, Z., Fazaeli, R., Fard, N.E., 2015. Monolayer and multilayer adsorption isotherm models for sorption from aqueous media. Korean J. Chem. Eng. 32, 787–799.

Sitko, R., Turek, E., Zawisza, B., Malicka, E., Talik, E., Heimann, J., Gagor, A., Feist, B., Wrzalik, R., 2013. Adsorption of divalent metal ions from aqueous solutions using graphene oxide. Dalt. Trans. 42, 5682–5689. https://doi.org/10.1039/C3DT33097D.

Sohi, S.P., Krull, E., Lopez-Capel, E., Bol, R., 2010. A review of biochar and its use and function in soil. Advances in Agronomy. Elsevier, pp. 47–82.

Song, J., He, Q., Hu, X., Zhang, W., Wang, C., Chen, R., Wang, H., Mosa, A., 2019. Highly efficient removal of Cr(VI) and Cu (II) by biochar derived from Artemisia argyi stem. Environ. Sci. Pollut. Res. 26, 13221–13234. https://doi.org/10.1007/s11356-019-04863-2.

Taheran, M., Naghdi, M., Brar, S.K., Verma, M., Surampalli, R.Y., 2018. Emerging contaminants: here today, there tomorrow! Environ. Nanotechnology, Monit. Manag. 10, 122–126. https://doi.org/10.1016/j.enmm.2018.05.010.

Vikrant, K., Kim, K.-H., 2018. Nanomaterials for the adsorptive treatment of Hg (II) ions from water. Chem. Eng. J. 358, 264–282.

Wang, Z., Yang, X., Qin, T., Liang, G., Li, Y., Xie, X., 2019. Efficient removal of oxytetracycline from aqueous solution by a novel magnetic clay–biochar composite using natural attapulgite and cauliflower leaves. Environ. Sci. Pollut. Res. 26, 7463–7475. https://doi.org/10.1007/s11356-019-04172-8.

Wathukarage, A., Herath, I., Iqbal, M.C.M., Vithanage, M., 2017. Mechanistic understanding of crystal violet dye sorption by woody biochar: implications for wastewater treatment. Environ. Geochem. Health https://doi.org/10.1007/s10653-017-0013-8.

Weber, K., Quicker, P., 2018. Properties of biochar. Fuel 217, 240–261. https://doi.org/10.1016/j.fuel.2017.12.054.

Wei, R., Ge, F., Huang, S., Chen, M., Wang, R., 2011. Occurrence of veterinary antibiotics in animal wastewater and surface water around farms in Jiangsu Province, China. Chemosphere 82, 1408–1414. https://doi.org/10.1016/j.chemosphere.2010.11.067.

WHO, 2012. Pharmaceuticals in Drinking-Water.

Xu, R., Xiao, S., Yuan, J., Zhao, A., 2011. Adsorption of methyl violet from aqueous solutions by the biochars derived from crop residues. Bioresour. Technol. 102, 10293–10298.